Acta Crystallographica Section B
Structural Science
ISSN 0108-7681

Dynamic proton disorder and the II–I structural phase transition in $(NH_4)_3H(SO_4)_2$

Yoo Jung Sohn,[a]* Anja Loose,[a] Michael Merz,[a,b] Karine Sparta,[a] Helmut Klapper[a] and Gernot Heger[a]

[a]RWTH Aachen University, Institut für Kristallographie, Jägerstrasse 17-19, 52056 Aachen, Germany, and [b]Forschungszentrum Karlsruhe, Institut für Festkörperphysik, Postfach 3640, 76021 Karlsruhe, Germany

Correspondence e-mail: sohn@xtal.rwth-aachen.de

Received 8 September 2008
Accepted 9 December 2008

X-ray powder diffraction, differential scanning calorimetry (DSC)/thermogravimetry (TG) and single-crystal neutron diffraction methods were used to investigate triammonium hydrogen disulfate $(NH_4)_3H(SO_4)_2$ (TAHS) in the temperature range between 293 and 493 K. The temperature-dependent X-ray powder diffraction measurements show a clear hysteresis of the I $\leftrightarrow$ II phase transition of TAHS with transition temperatures of T_{up} = 412.9 (1) K on heating and of T_{down} = 402.6 (1) K on cooling. From the existence of hysteresis and from the jump-like changes of the lattice parameters, the I $\leftrightarrow$ II phase transition of TAHS is considered to be first order. With DSC/TG measurements we confirmed that there is only one phase transition between 293 and 493 K. Through careful investigation on single crystals of TAHS using neutron diffraction, the correct space group ($C2/c$) of room-temperature TAHS-II phase was confirmed. Crystal structure analysis by single-crystal neutron diffraction showed a strongly elongated displacement ellipsoid of the proton which lies in the middle of the $(SO_4)H(SO_4)$ dimer with $\bar{1}$ local symmetry. The protons of the NH_4 groups also show strongly enlarged anisotropic mean-square displacements. These findings are interpreted in terms of a characteristic proton disorder in the TAHS-II phase.

1. Introduction

Triammonium hydrogen disulfate $(NH_4)_3H(SO_4)_2$ (TAHS) belongs to the well known family of compounds with the general formula $M_3H(XO_4)_2$ ($M = NH_4^+, K^+, Rb^+, Cs^+$; X = S, Se). These compounds are characterized by the strong hydrogen bond between two XO_4^{2-} ions forming a $(XO_4)H(XO_4)$ dimer. For a few decades there has been a continuous interest in studying TAHS for its rich polymorphism involving six different phases (Gesi, 1976) and for its superprotonic conductivity in its high-temperature phase (Chen *et al.*, 2000). The series of phase transitions is shown in the following with its denotation and phase transition temperatures

$$\text{VI} \overset{63\,\text{K}}{\longleftrightarrow} \text{V} \overset{133\,\text{K}}{\longleftrightarrow} \text{IV} \overset{141\,\text{K}}{\longleftrightarrow} \text{III} \overset{265\,\text{K}}{\longleftrightarrow} \text{II} \overset{413\,\text{K}}{\longleftrightarrow} \text{I}.$$

Phase I is paraelastic and phase II is ferroelastic. Crystal structure analysis of TAHS in phases I, II, III, IV and V have only been performed so far by single-crystal X-ray diffraction (Swain & Row, 2007; Dominiak *et al.*, 2003; Friese *et al.*, 2002). However, the proton disorder in the hydrogen bond of the $(SO_4)H(SO_4)$ dimer and of the NH_4 groups cannot be described sufficiently with X-ray diffraction methods. Since the understanding of the hydrogen ordering is of fundamental importance to explain the mechanisms of the phase transitions of TAHS, we performed neutron diffraction studies on single

crystals. Moreover, we carried out a careful investigation regarding the space-group symmetry of TAHS in its room-temperature phase II, because an ambiguity exists concerning the correct space-group symmetry of TAHS-II (Tamura *et al.*, 1999).

Another aspect concerns the existence of additional phase transitions of TAHS. In the literature, Chen *et al.* (2000) and Fukami *et al.* (1994) reported on anomalies from impedance spectroscopy and DSC measurements at 433 and at 463 K, respectively, which were interpreted as new phase transitions above room temperature. We performed detailed X-ray powder diffraction studies and DSC/TG measurements in order to verify these results.

2. Experimental

2.1. Crystal growth and powder sample preparation

Single crystals of TAHS were grown from aqueous solution both by slow evaporation and by the temperature-cooling method. Transparent platelet-like crystals were grown with a dominant face of (001) and a pseudo-hexagonal habitus. The quality of powder samples plays a significant role not only for X-ray and DSC measurements but also for other physical studies, since it can affect the results of the experiments. We first tried to obtain powder samples of TAHS through precipitation in acetone. However, the X-ray powder diffractograms showed that these samples were not single phase. To obtain single-phase powder samples, single crystals of TAHS were ground. Powders which were ground under normal conditions in an agate mortar in air yield single-phase X-ray powder diffraction patterns of TAHS-II with, in addition, some enhanced and structured backgrounds. On heating a dramatic increase of Bragg-peak intensities was observed, which could be attributed to a recrystallization of water-containing minor phases on the surface of the platelet-like powder grains. We assumed that these minor phases were caused by pressure and atmospheric humidity during the grinding process. Fig. 1 shows a section of complete powder patterns which were repeatedly recorded at a constant temperature of 367.5 (1) K (1 h each). As shown in the diagram, there is an increase of reflection intensities, but no change of the reflection positions. Stable conditions were achieved after *ca* 3 h. These preparation-induced phenomena were avoided by grinding single crystals in a glovebox under a dry atmosphere (relative humidity in the range $\sim$ 0.4–1.2%).

The ground powder samples of TAHS show in general a pronounced texture, which is increased by surface recrystallization depending on the sample preparation. In order to confirm that the powder samples of TAHS were strongly textured, we performed an X-ray diffraction measurement with a two-dimensional image-plate detector. The powder samples were thereby introduced into a capillary with a diameter of 0.7 mm. In Fig. 2 the texture effect is clearly visible by the powder rings decorated with distinct reflections.

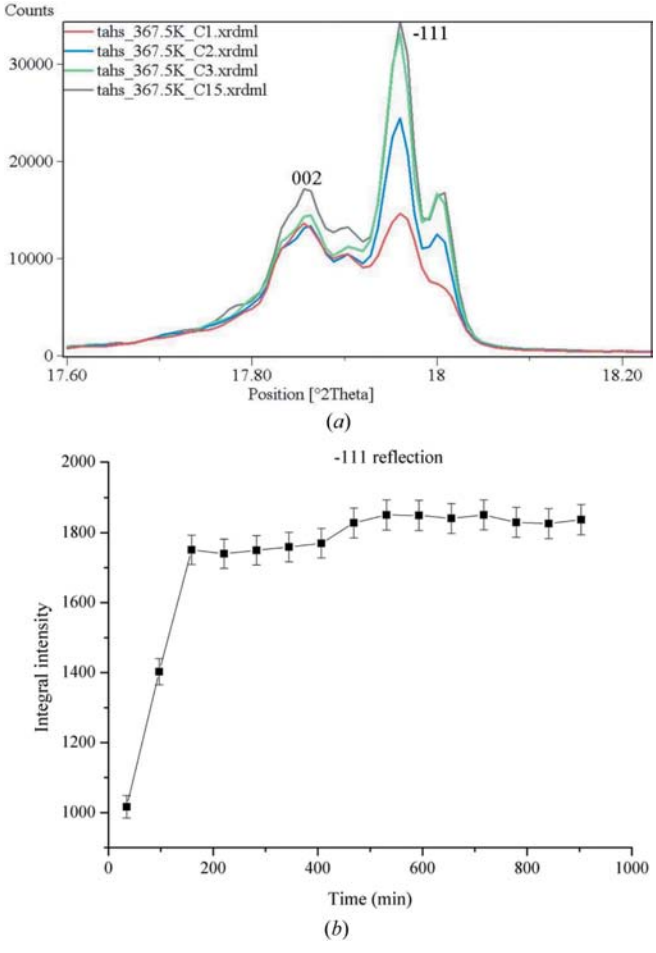

Figure 1
(*a*) A section of repeated X-ray powder diffraction patterns of ground crystals in air at a fixed temperature of 367.5 (1) K. (*b*) Integral intensity of the $\bar{1}11$ reflection as a function of time.

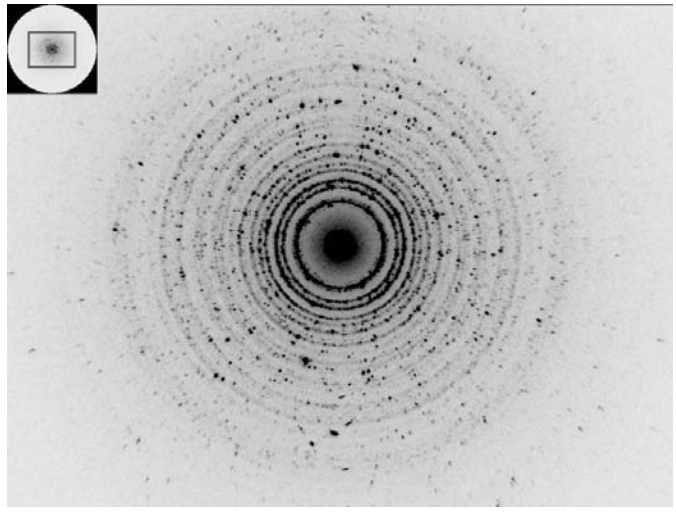

Figure 2
Powder diffraction pattern recorded with a two-dimensional image-plate detector (IPDS 2 Stoe) perpendicular to the incident monochromated X-ray beam (Mo $K\alpha$). The powder rings are decorated by distinct reflections, which clearly show the texture problem of the sample.

Table 1
Experimental and refinement details of single-crystal neutron diffraction.

	Conventional model	Split-atom model
Crystal data		
Chemical formula	$HO_8S_2\cdot 3H_4N$	$HO_8S_2\cdot 3H_4N$
M_r	247.25	247.25
Cell setting, space group	Monoclinic, *C*2/*c*	Monoclinic, *C*2/*c*
Temperature (K)	293 (2)	293 (2)
a, *b*, *c* (Å)	15.429 (8), 5.861 (3), 10.167 (5)	15.429 (8), 5.861 (3), 10.167 (5)
β (°)	101.83 (5)	101.83 (5)
V (Å^3)	899.9 (8)	899.9 (8)
Z	4	4
D_x (Mg m^{-3})	1.825	1.825
Radiation type	Neutron	Neutron
μ (mm^{-1})	0.22	0.22
Crystal form, colour	Cuboid, white	Cuboid, white
Crystal size (mm)	3 × 3 × 3	3 × 3 × 3
Data collection		
Diffractometer	Four-circle	Four-circle
Data collection method	ω scan	ω scan
Absorption correction	None	None
No. of measured, independent and observed reflections	1169, 1143, 770	1169, 1143, 770
Criterion for observed reflections	$I > 2\sigma(I)$	$I > 2\sigma(I)$
R_{int}	0.039	0.039
θ_{max} (°)	37.5	37.5
No. and frequency of standard reflections	2 every 600 min	2 every 600 min
Intensity decay (%)	0	0
Refinement		
Refinement on	F^2	F^2
$R[F^2>2\sigma(F^2)]$, $wR(F^2)$, S	0.094, 0.144, 1.97	0.094, 0.144, 1.98
No. of reflections	1143	1143
No. of parameters	120	118
H-atom treatment	Refined independently	Refined independently
Weighting scheme	$w = 1/[\sigma^2(F_o^2) + 7P]$, where $P = (F_o^2 + 2F_c^2)/3$	$w = 1/[\sigma^2(F_o^2) + 7P]$, where $P = (F_o^2 + 2F_c^2)/3$
$(\Delta/\sigma)_{max}$	< 0.0001	< 0.0001
$\Delta\rho_{max}$, $\Delta\rho_{min}$ (e Å^{-3})	1.07, −1.24	1.11,−1.24

Computer programs used: *DIF4N* (Stoe & Cie, 1991), *PRON* (Scherf, 1998), *SHELXL*97 (Sheldrick, 2008), *ATOMS* (Dowty, 2000).

2.2. X-ray powder diffraction

X-ray powder diffraction patterns were recorded with an X'pert PRO diffractometer (PANalytical). The data were collected in Bragg–Brentano geometry using Cu $K\alpha_{1,2}$ radiation. Owing to the θ–θ geometry of the diffractometer, the flat sample stayed fixed in the horizontal plane. The intensity was recorded by a position-sensitive detector (X'Celerator, PANalytical). For the high-temperature measurements a specially developed furnace was used where the platinum heater serves at the same time as the sample holder. The temperature of the sample was controlled by a NiCr–Ni thermocouple in direct contact with the platinum heater, and a stability of ± 0.1 K was achieved. A Si standard was added to the powder sample of TAHS to correct for changes in sample geometry with temperature. Diffraction patterns were measured at various temperatures in a step-like manner between 297.4 (1) and 427.4 (1) K in the 2θ range from 10 to 90° with $\Delta 2\theta$ = 0.008°. At each temperature the complete powder patterns recorded in ∼1 h were repeated several times in order to control the stability of the measurements. There were no significant changes between these complete powder patterns collected at a fixed temperature. A strong texture effect occurred owing to the plate-like shape of the crystal grains (see Fig. 2). Therefore, only profile-matching of the data by the *FULLPROF* program (Rodriguez-Carvajal, 2001) and no Rietveld refinement was performed.

2.3. DSC/TG

The DSC/TG measurements were performed with a Netzsch STA 409 apparatus in the temperature range between 293.0 (5) and 493.0 (5) K. The heating and the cooling rate of 3 K min^{-1} was chosen, because the time-dependent thermal decomposition is not visible under these conditions up to 493.0 (5) K. To verify whether the results were reproducible, experiments were repeated under the same conditions. It was also checked with the DSC/TG method if there is more than one phase transition above room temperature.

2.4. Single-crystal neutron diffraction

Single-crystal neutron diffraction studies were performed at room temperature on the four-circle diffractometer SV28 at the research reactor DIDO/FZ-Jülich with a wavelength of λ = 0.87238 (5) Å [Cu(220) monochromator]. A complete dataset of Bragg reflection intensities was collected up to $(\sin\theta/\lambda)_{max}$ = 0.7 Å^{-1} using a single crystal of 3 × 3 × 3 mm^3. Data reduction was performed with the program *PRON* (Scherf, 1998). The structure refinement was carried out with the *SHELXL*97 program (Sheldrick, 2008). The experimental details are given in Table 1.[1]

3. Results and discussion

3.1. X-ray powder diffraction

The purpose of the X-ray powder measurements was firstly to determine the lattice parameters of TAHS in the room- and high-temperature phases and to check whether more than one phase transition exists above room temperature. As described in §2.1, TAHS single crystals were ground with Si standard and

[1] Supplementary data for this paper are available from the IUCr electronic archives (Reference: GW5001). Services for accessing these data are described at the back of the journal.

Table 2
Crystallographic data of TAHS from powder X-ray diffraction measurements in phases TAHS-II and TAHS-I.

Phase	TAHS-II	TAHS-I
Cell setting, space group	Monoclinic, $C2/c$	Hexagonal, $R\bar{3}m$
Temperature (K)	297	423
a, b, c (Å)	15.431 (8), 5.861 (3), 10.169 (5)	5.907 (3), 5.907 (3), 22.57 (1)
β (°)	101.83 (5)	–
V (Å^3)	900.2 (5)	682.1 (3)
Z	4	3
D_x (Mg m^{-3})	1.824	1.806

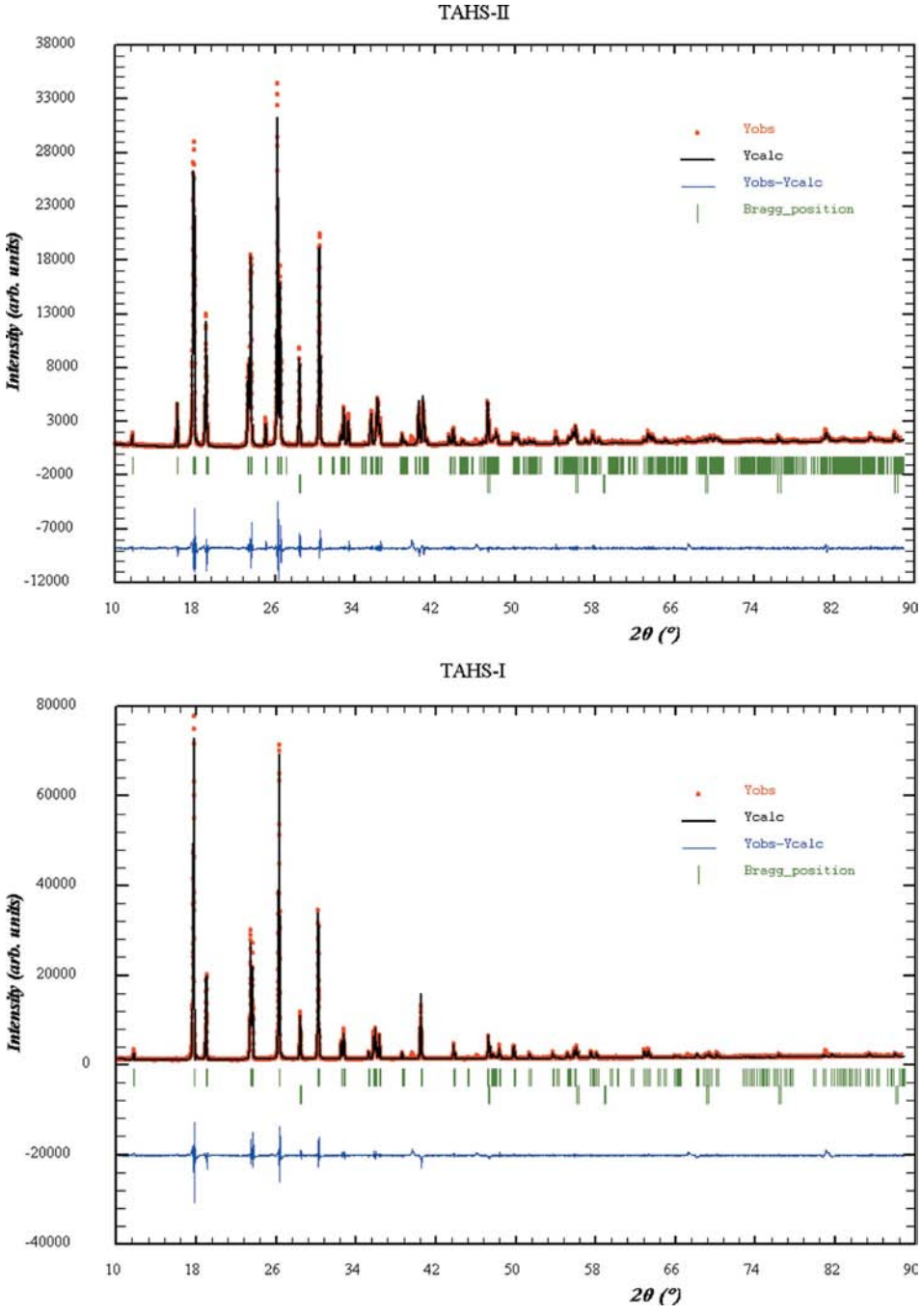

Figure 3
Profile-matching of TAHS-II and TAHS-I phases with Si standard at 297.4 (1) and at 427.4 (1) K, respectively.

immediately placed on a sample holder in a glovebox under a dry atmosphere. Powder samples obtained in this way yield a single-phase TAHS-II diffractogram of good quality which does not change with time. When heating from room temperature up to 427.4 (1) K followed immediately by cooling back to 297.4 (1) K, we obtained reproducible powder patterns concerning the peak positions, line shapes and intensities. Only one phase transition was observed above room temperature. The crystallographic data of TAHS-II and TAHS-I phases are summarized in Table 2.

The results of the profile-matching refinements of TAHS-II and TAHS-I are shown in Fig. 3. The lattice parameters and unit-cell volume of TAHS as a function of temperature are presented in Fig. 4. The data of the rhombohedral high-temperature phase TAHS-I were converted to the monoclinic lattice of the room-temperature structure TAHS-II ($\boldsymbol{a}_m = \frac{2}{3}\boldsymbol{a}_r + \frac{1}{3}\boldsymbol{b}_r - \frac{2}{3}\boldsymbol{c}_r$, $\boldsymbol{b}_m = -\boldsymbol{b}_r$, $\boldsymbol{c}_m = \boldsymbol{c}_r$) for a better comparison. From the jump of the a, b, β lattice parameters, the unit-cell volume of TAHS and from the observed hysteresis, the I $\leftrightarrow$ II phase transition of TAHS can be characterized as a first-order phase transition. A possible group–subgroup relation between the TAHS-I and TAHS-II phases exists

$$R\bar{3}m\,(\text{TAHS-I}) \overset{\text{k[2]}}{\longleftrightarrow} R\bar{3}c\,(\boldsymbol{c}' = 2\boldsymbol{c}) \overset{\text{t[3]}}{\longleftrightarrow} C12/c1\,(\text{TAHS-II}).$$

which is combined with a doubling of the c lattice parameter. The temperature-dependent intensity of the 110 reflection of the monoclinic TAHS-II phase, which disappears in the rhombohedral TAHS-I phase, confirmed the I $\leftrightarrow$ II phase transition (Fig. 5). The integral intensity of this relatively weak reflection, which is strongly affected by the background correction, is more or less constant up to the

phase transition. There is a clear hysteresis of ~ 10 K with transition temperatures of $T_{up} = 412.9$ (1) K upon heating and of $T_{down} = 402.6$ (1) K upon cooling.

Owing to the high quality and reproducibility of our X-ray powder diffraction measurements on TAHS, we are able to show that the background of the powder patterns changes significantly with temperature. In Fig. 6 the background decreases continuously with decreasing temperature from 427.4 (1) to 297.4 (1) K with a significant step at the phase transition temperature. An increased background resulting from diffuse scattering can be attributed to structural disorder. Although phases TAHS-I and TAHS-II are both dynamically disordered, it becomes obvious that the degree of disorder is reduced considerably when passing from the high-temperature superprotonic TAHS-I to the TAHS-II room-temperature phase. Moreover, there is a continuous decrease of disorder in the monoclinic TAHS-II phase with decreasing temperature.

Since the contribution of the H atoms to the X-ray diffraction intensity is rather small, it can be assumed that the diffuse background scattering does not only originate from the H atoms but additionally from contributions of the hydrogen-linked $(SO_4)H(SO_4)$ dimers. The peak shape of the Bragg reflections is well established according to the resolution function of the instrument and does not change significantly as a function of temperature for the two phases TAHS-II and TAHS-I.

The dynamical disorder of the protons of the NH_4 groups and the $(SO_4)H(SO_4)$ dimers in TAHS were recently studied by Fechtelkord *et al.* (2007) using NMR techniques. They confirm an increase of proton dynamics within the $(SO_4)H(SO_4)$ dimer in the TAHS-II phase when approaching the I $\leftrightarrow$ II transition, with a major change at the phase transition temperature. The coexistence range of the ferro- and paraelastic phases of ~ 15 K corresponds to the hysteresis width of our experiments of ~ 10 K.

3.2. DSC/TG

When the powder sample of TAHS was ground and prepared under normal conditions in air, we could observe a continuous falling of the TG line as the temperature increased (Fig. 7). However, the powder sample which had been prepared in a glovebox showed a constant TG line (Fig. 8). This is in accordance with our X-ray powder diffraction results (§2.1). The weight loss is due to the evaporation of H_2O on heating.

Using the DSC/TG measurements with a powder sample of TAHS which was heated slightly above the phase transition temperature up to 423.0 (5) K and then immediately cooled down, we could observe only one phase transition with an endothermic signal at 413.5 (5) K on heating and at 412.5 (5) K on cooling with an exothermic signal (Fig. 8). A second heating/cooling cycle showed almost the same transition temperatures and no additional anomalies.

On the other hand, when the sample was heated up to 493.0 (5) K, kept at this temperature for 2 h and cooled down again, we observed many new peaks on cooling (Fig. 9), which were not reproducible. We interpret our results in the context of thermal decomposition at temperatures above the structural phase transition. We also observed from X-ray powder diffraction that after heating for several hours in the

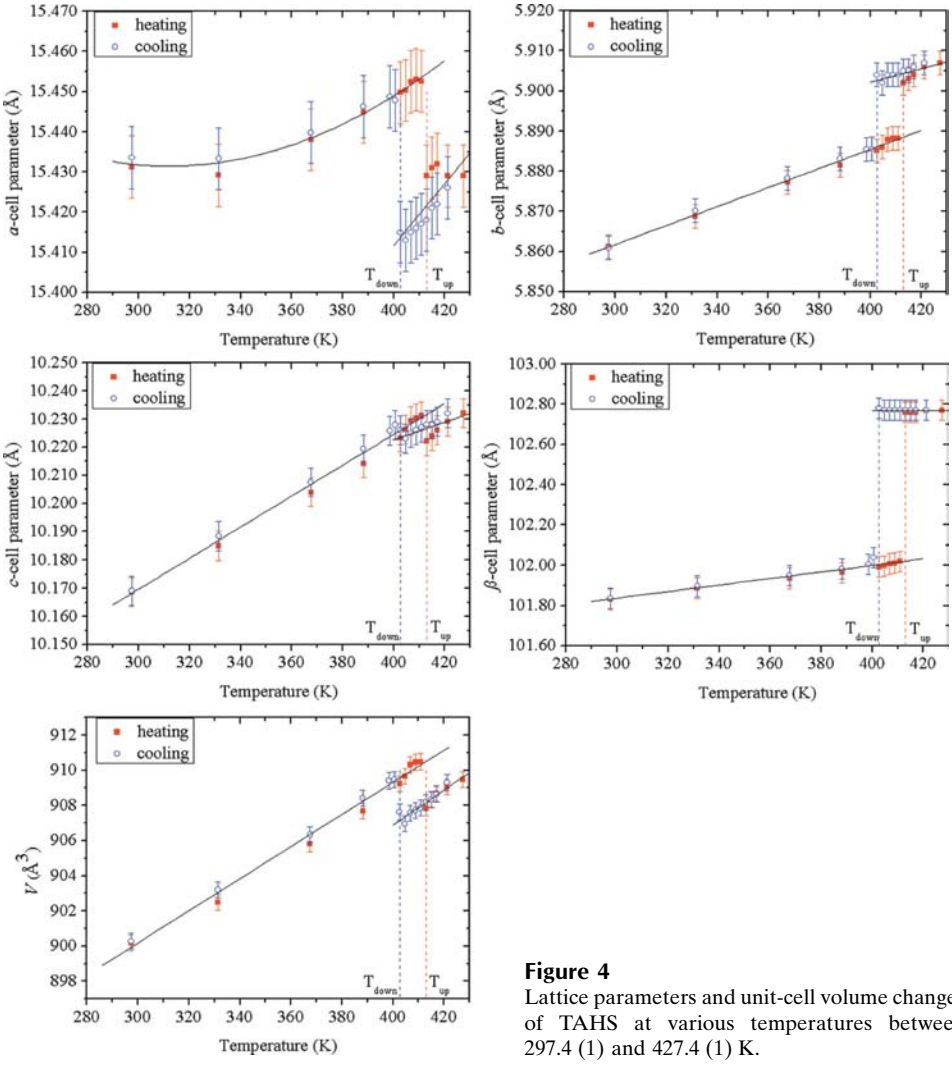

Figure 4
Lattice parameters and unit-cell volume changes of TAHS at various temperatures between 297.4 (1) and 427.4 (1) K.

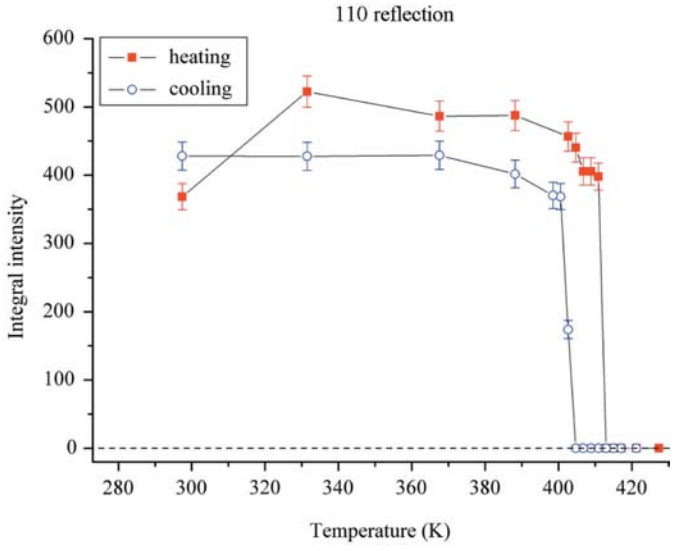

Figure 5
Temperature-dependent integral intensity of the 110 reflection on heating and cooling.

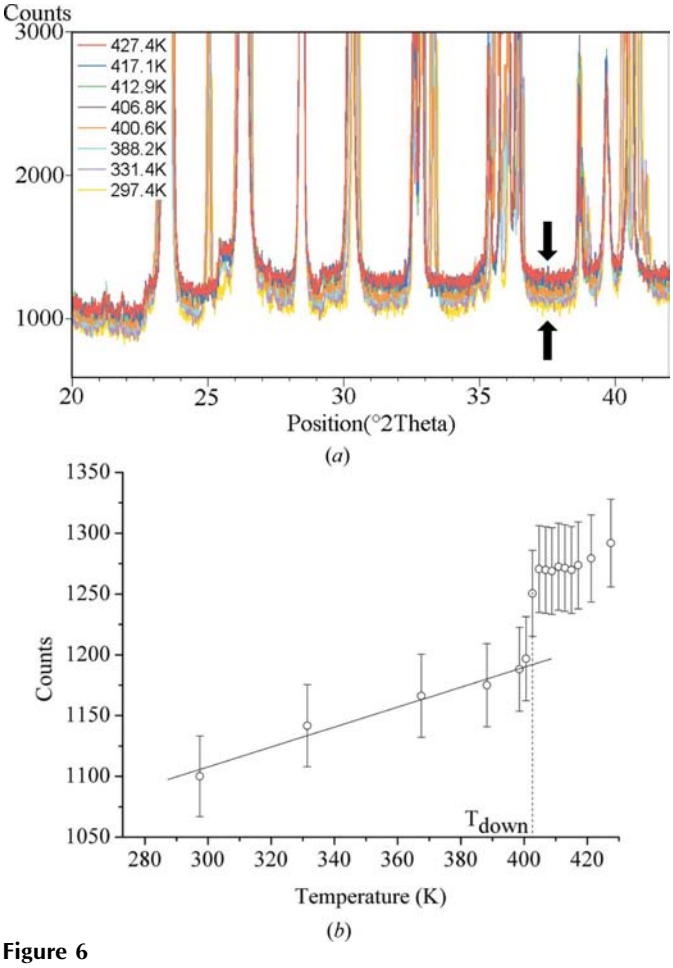

Figure 6
Decrease of the background intensity from the high-temperature phase TAHS-I at 427.4 (1) K to the room-temperature phase TAHS-II at 297.4 (1) K. (*a*) An enlarged section of the diffraction pattern between $20 \leq 2\theta \leq 42^\circ$. (*b*) Background intensity averaged over the 2θ range from 37 to 38° (according to the arrows in *a*) as a function of temperature.

high-temperature phase the sample showed additional peaks and broadening of peak lines, which indicated that the sample was no longer single phase. These additional peaks could be attributed to $(NH_4)H(SO_4)$ (Nelmes, 1971). With the DSC measurements we confirmed that there is only one phase transition in the temperature range up to 493.0 (5) K. This is valid for powder samples prepared under dry conditions (Fig. 8) as well as normal conditions (Fig. 7). The other two phase transitions above room temperature mentioned in the literature were reportedly found when the sample was heated with a very low heating rate (1 and 0.1 K min^{-1} around the phase transition temperature by Chen *et al.*, 2000, and 0.25 K min^{-1} by Fukami *et al.*, 1994). As it is unknown whether those heating experiments were followed by cooling measurements and additional heating/cooling cycles, the question of a possible thermal decomposition of the sample still remains.

3.3. Single-crystal neutron diffraction

3.3.1. Space-group symmetry of the TAHS-II phase. There exists some controversy concerning the 'true' space-group symmetry of the room-temperature phase of TAHS-II. The majority of papers in the literature supports the choice of centrosymmetric space group $C12/c1$ (No. 15) in the conventional setting of the *International Tables for Crystallography* (Hahn, 2002) with lattice parameters $a_C = 15.431$ (8), $b_C = 5.861$ (3), $c_C = 10.169$ (5) Å and $\beta_C = 101.83$ (5)° (Swain & Row, 2007; Dominiak *et al.*, 2003; Friese *et al.*, 2002). In older publications a different choice of basis vectors (*viz.* interchange of basis vectors $\boldsymbol{a}$ and $\boldsymbol{c}$) of the lattice led to the space-group symbol $A2/a$ (in full notation $A12/a1$) with $\boldsymbol{a}_A = \boldsymbol{c}_C$, $\boldsymbol{b}_A = -\boldsymbol{b}_C$ and $\boldsymbol{c}_A = \boldsymbol{a}_C$ (Suzuki & Makita, 1978). This space-group notation should not be confused with $A2/a$ of *International Tables for Crystallography* (Hahn, 2002; in full notation $A112/a$) with the monoclinic unique axis c and $\boldsymbol{a}'_A = \boldsymbol{c}_C$, $\boldsymbol{b}'_A = \boldsymbol{a}_C$, and $\boldsymbol{c}'_A = \boldsymbol{b}_C$.

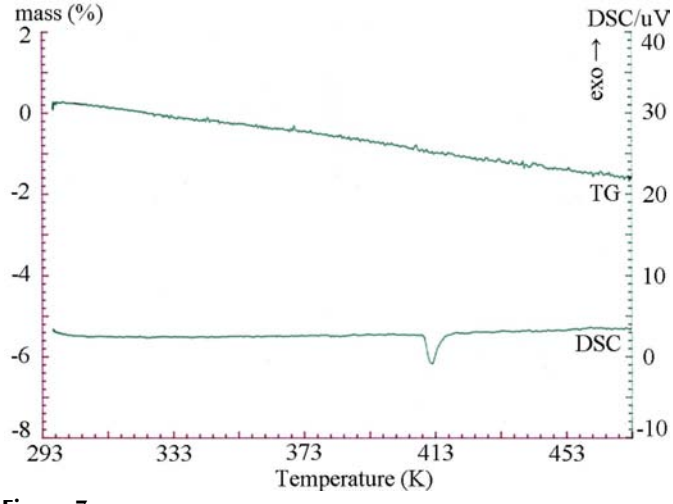

Figure 7
DSC/TG measurements of powder samples of TAHS prepared under 'normal' conditions. TG decreases continuously as the temperature rises. There is only one phase transition at 412.4 (5) K on heating up to 473.0 (5) K.

Table 3
Reflection conditions for space groups $C12/c1$, $A12/a1$ and $A112/a$.

Reflections	$C12/c1$	$A12/a1$	$A112/a$
hkl	$h+k=2n$	$k+l=2n$	$k+l=2n$
$h0l$	$h, l=2n$	$h, l=2n$	$l=2n$
$0kl$	$k=2n$	$k+l=2n$	$k+l=2n$
$hk0$	$h+k=2n$	$k=2n$	$h, k=2n$

In diffraction experiments the space groups $C12/c1$, $A12/a1$ and $A112/a$ yield the conditions for possible Bragg reflections as given in Table 3.

Tamura *et al.* (1999) have investigated the question of the existence (or not) of centrosymmetry for TAHS-II and the isostructural fully deuterated TADS-II by neutron diffraction experiments on single crystals. They concluded from the violation of the reflection conditions for $A2/a$ that the non-centrosymmetric space group $A2$ is correct. In their paper there is no direct indication of their choice of basis vectors. Information on space-group setting, monoclinic unique axis or lattice parameters are missing. From the cited papers and from their argumentation on the extinction conditions of the *a* glide symmetry for the $h0l$ reflections, one can assume that they have chosen the same space-group settings $A12/a1$ and $A121$, respectively, as Suzuki & Makita (1978).

We have performed now for the first time a complete structure analysis of TAHS-II by single-crystal neutron diffraction at room temperature. In order to check the reflection conditions according to the space groups $C12/c1$ and $C121$, all hkl reflections were measured up to $\sin\theta/\lambda = 0.4$ Å^{-1}. Without any exceptions we confirm the centrosymmetric space group $C12/c1$ (and hence also its transformed setting $A12/a1$).

Tamura *et al.* (1999) performed their neutron diffraction studies on rather large crystals of volume ~ 360 mm^3 and argued that the 'forbidden' reflections by the *a* glide symmetry have intensities more than a 100 times smaller than 'funda-

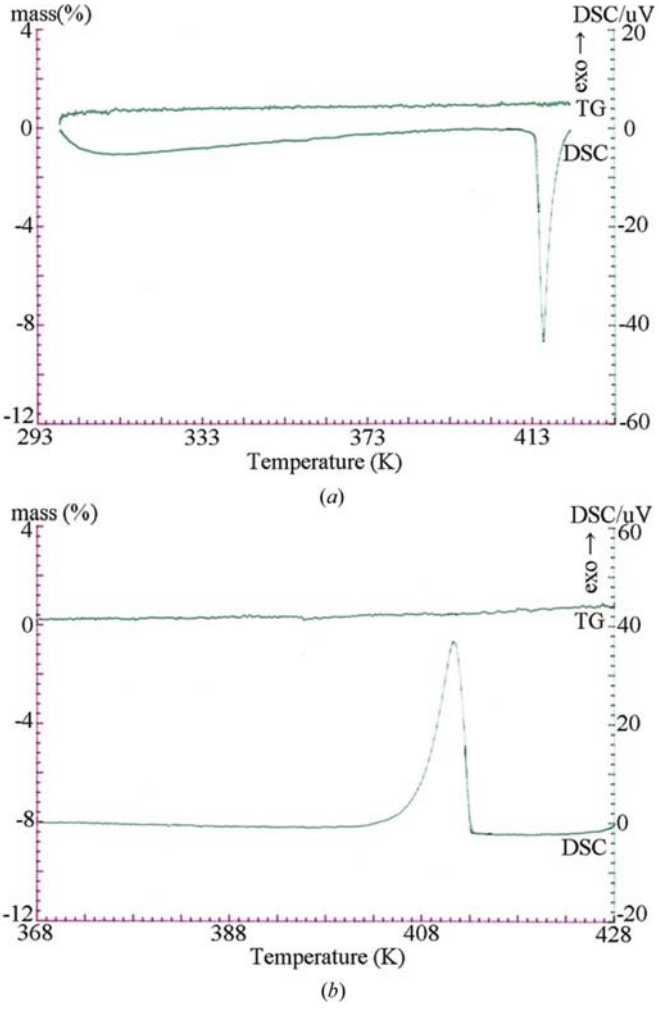

Figure 8
DSC/TG measurements of powder samples of TAHS prepared under 'dry' conditions. The mass stays constant during the measurements (*a*) on heating and (*b*) on cooling.

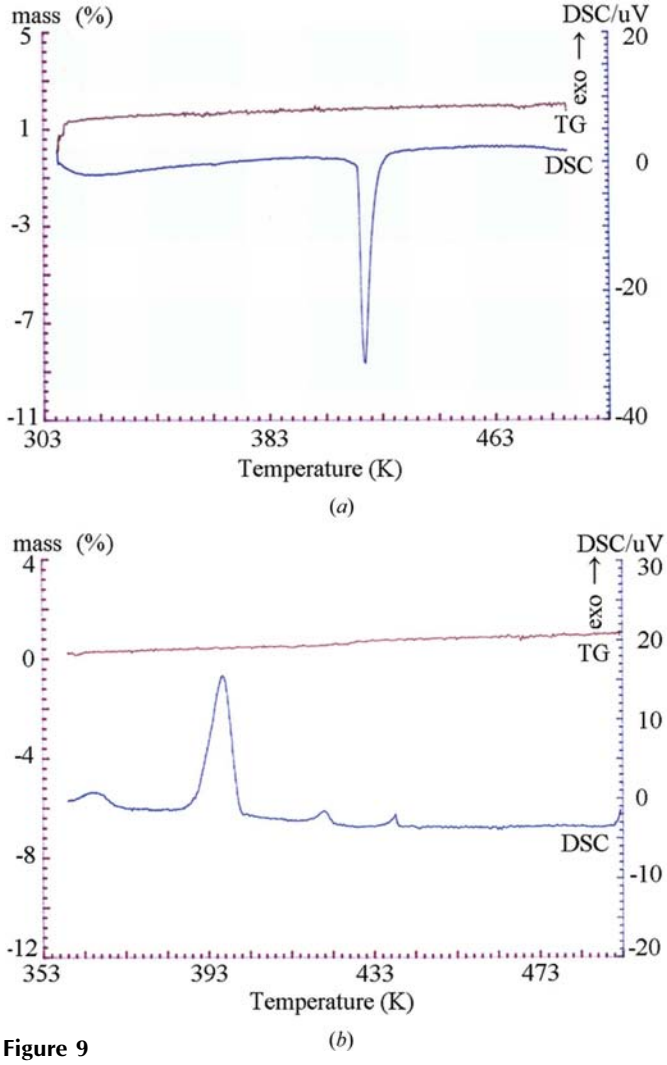

Figure 9
DSC/TG measurements of powder samples of TAHS prepared under 'dry' conditions. (*a*) Only one phase transition at 413.5 (5) K on heating up to 493.0 (5) K. (*b*) Many new anomalies on cooling after 2 h at 493.0 (5) K.

mental' Bragg reflections. Therefore, we repeated neutron diffraction measurements with a large crystal of 6 × 7 × 8 mm^3 on selected $h0l$ reflections with $l = 2n + 1$ (the reflection condition for the space group $C12/c1$ is $l = 2n$) and found no indication of significant intensities within a ratio of at least 1000 compared with strong Bragg reflections.

We have not been able to confirm the results of Tamura *et al.* (1999) and we have no satisfying explanation for this disagreement. There is a possibility that extinct reflections due to symmetry operations with translation components like glide reflections or screw rotations may occur by multiple diffraction. This so-called Renninger effect depends strongly on the diffraction geometry of the crystal and becomes more important when using large (and perfect) single crystals. We tried to find Renninger-effect intensities for selected $h0l$ reflections with $l = 2n + 1$ by the ψ-scan technique, but again no indication was obtained. On the other hand, it is important to stress that the choice of basis vectors and space groups of Tamura *et al.* (1999) remains an open question.

The discussion on the space-group symmetry of TAHS-II is of great importance for the crystal structure analysis. Our model of a highly disordered proton distribution in the O—H···O hydrogen bonds of the $(SO_4)H(SO_4)$ dimers and the N—H···O bonds between the NH_4 groups and the nearby SO_4 groups is directly related to the existence of centres of symmetry in the structure.

3.3.2. Room-temperature structure. As described above, we refer to the correct space-group symmetry of the room-temperature phase of TAHS-II as $C2/c$. At the beginning of the refinement every atom including H atoms was refined with anisotropic mean-square displacement parameters. The H1 atom in the middle of the $(SO_4)H(SO_4)$ dimer lies on an inversion centre. Its displacement ellipsoid is strongly elongated in the direction of the symmetric O···H···O bonding and the O1···H1 distance is unusually long [1.27 (1) Å].

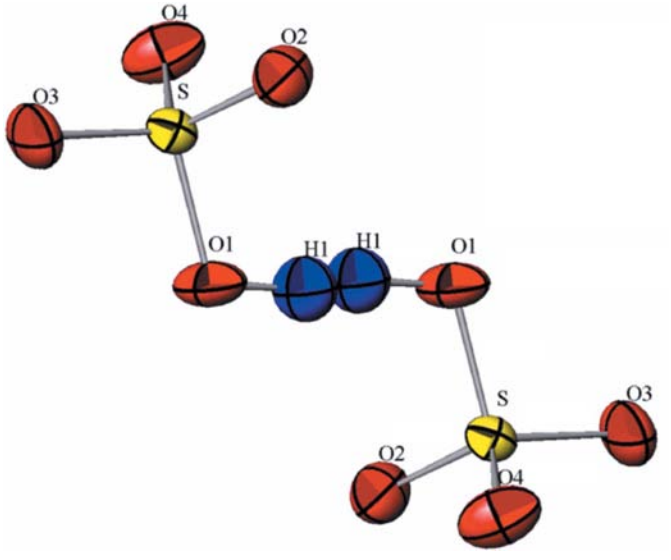

Figure 10
$(SO_4)H(SO_4)$ dimer with a split position for H1. Displacement ellipsoids are drawn at the 50% probability level.

Table 4
Bond lengths (Å) of $(SO_4)H(SO_4)$ dimer (split-atom model).

S—O1	1.526 (5)
S—O2	1.434 (7)
S—O3	1.457 (6)
S—O4	1.446 (6)
O1—H1	0.99 (1)
O1—O1	2.549 (7)

Because of this peculiar behaviour, we chose for the next refinement a split model with isotropic displacements to describe the hydrogen distribution within the dimer. Our results support the earlier assumption of a split position for H1 based on single-crystal X-ray diffraction data (Dominiak *et al.*, 2003). The covalent character of the O1···H1 bond causes an electronic transfer from the S—O1 bond to the O1···H1 bond. This results in a significant lengthening of the weakened S—O1 bond compared with the other S—O bonds. The result of this refinement is shown in Fig. 10 and the bond lengths are given in Table 4.

Furthermore, the H atoms of the two non-equivalent NH_4 groups also have strongly enlarged anisotropic mean-square displacements. This enlargement is presumably caused by a jump-like motion between different NH_4 orientations. The N atoms of both NH_4 tetrahedral groups are well localized with small, almost isotropic mean-square displacement parameters. We can attribute two possible oxygen neighbours for each hydrogen from the SO_4 groups (Figs. 11 and 12), which leads to a system of competing N—H···O hydrogen bonds between the NH_4 groups and the surrounding O atoms and thus to a

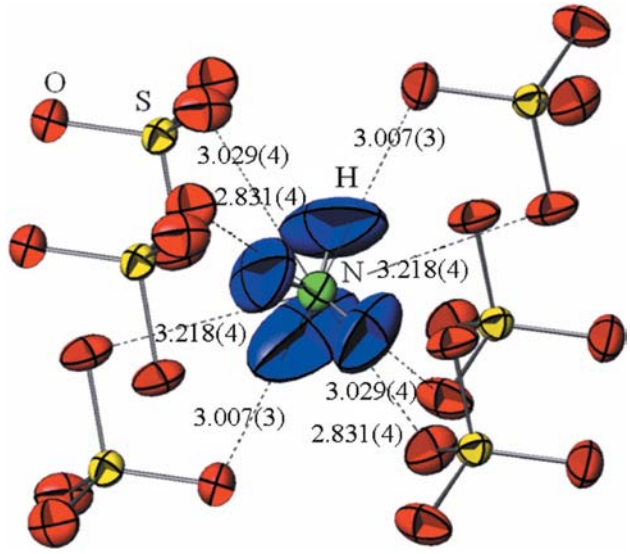

Figure 11
$N1H_4$ tetrahedron with neighbouring SO_4 groups. Displacement ellipsoids are drawn at the 50% probability level. The mean value of the interatomic distances between N1 and the eight surrounding O atoms is 3.021 (4) Å.

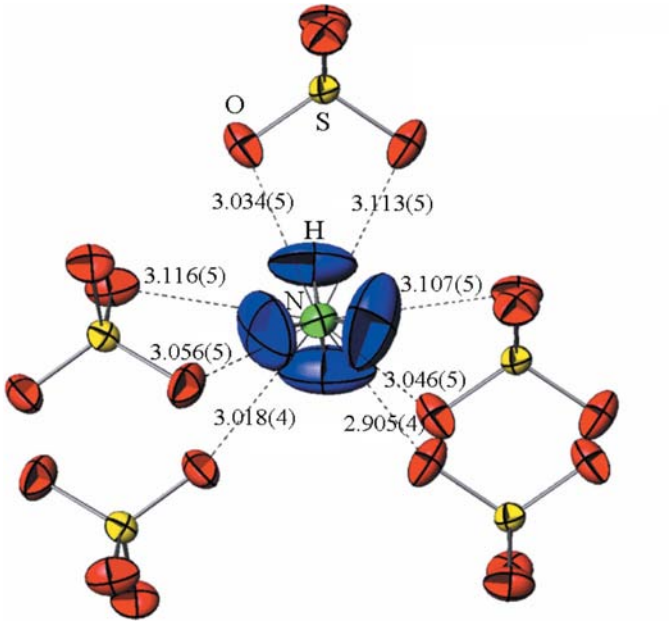

Figure 12
$N2H_4$ tetrahedron with neighbouring SO_4 groups. Displacement ellipsoids are drawn at the 50% probability level. The mean value of the interatomic distances between the N2 and the eight surrounding O atoms is 3.049 (5) Å.

rotation of the NH_4 groups, in agreement with the fast dynamic reorientation of these tetrahedra reported by Fechtelkord *et al.* (2007). The distribution of H atoms in Figs. 11 and 12 is to be understood as a time- and space-averaged representation. The interatomic distances between the N and the O atoms of the possible N—H···O hydrogen bonds are also given. The S atoms also show almost isotropic mean-square displacements like the N atoms, whereas the O atoms exhibit significantly anisotropic displacement. The SO_4 groups are well defined within the $(SO_4)H(SO_4)$ dimer, however, they may perform librational motion in relation to the NH_4 disorder.

4. Conclusions

We have shown that experimental results on TAHS powder samples depend strongly on the preparation conditions. With our X-ray powder diffraction and DSC/TG measurements, we confirm that there is only one phase transition of TAHS in the temperature range between room temperature and 493 K. The phase transition between the monoclinic TAHS-II and the rhombohedral TAHS-I at *ca* 413 K is of first order with a hysteresis of *ca* 10 K. From the structure analysis based on single-crystal neutron diffraction data of TAHS-II at room temperature, we ascertained unequivocally that the correct space group is $C2/c$. We have clear evidence for a dynamical proton disorder in the $(SO_4)H(SO_4)$ dimer as well as in the NH_4 groups. We interpret the NH_4 dynamics as resulting from competing N—H···O hydrogen bonds. The dynamical proton disorder becomes more important with increasing temperature. In agreement with the NMR results of Fechtelkord *et al.* (2007) we consider a principal change at the phase transition to the superprotonic TAHS-I phase. The extremely disordered crystal structure of rhombohedral TAHS-I phase is under investigation by single-crystal neutron diffraction.

References

Chen, R. H., Chen, T. M. & Shern, C. S. (2000). *J. Phys. Chem. Solids*, **61**, 1399–1406.
Dominiak, P. M., Herold, J., Kolodziejski, W. & Woźniak, K. (2003). *Inorg. Chem.* **42**, 1590–1598.
Dowty, E. (2000). *ATOMS*, Version 5.1. Shape Software, Kingsport, USA.
Fechtelkord, M., Diekmann, A. & Bismayer, U. (2007). *Am. Mineral.* **92**, 1821–1832.
Friese, K., Aroyo, M. I., Schwalowsky, L., Adiwidjyjy, G. & Bismayer, U. (2002). *J. Solid State Chem.* **165**, 136–147.
Fukami, T., Tobaru, K., Kaneda, K., Nakasone, K. & Furukawa, K. (1994). *J. Phys. Soc. Jpn*, **63**, 2006–2007.
Gesi, K. (1976). *Phys. Status Solidi*, **33**, 479–482.
Hahn, Th. (2002). *International Tables for Crystallography*, Vol. A. Dordrecht: Kluwer Academic Publishers.
Nelmes, R. J. (1971). *Acta Cryst.* B**27**, 272–281.
Rodriguez-Carvajal, J. (2001). *CPD Newsl.* **26**, 12–19.
Scherf, C. (1998). *PRON*, Revised Stoe Version. Institute of Crystallography, Aachen, Germany.
Sheldrick, G. M. (2008). *Acta Cryst.* A**64**, 112–122.
Stoe & Cie (1991). *DIF4N*. Stoe & Cie, Darmstadt, Germany.
Suzuki, S. & Makita, Y. (1978). *Acta Cryst.* B**34**, 732–735.
Swain, D. & Row, T. N. G. (2007). *Inorg. Chem.* **46**, 4411–4421.
Tamura, I., Noda, Y. & Morii, Y. (1999). *J. Phys. Chem. Solids*, **60**, 1411–1414.